

Off-axis emission of short γ -ray bursts and the detectability of electromagnetic counterparts of gravitational wave detected binary mergers

Davide Lazzati¹, Alex Deich², Brian J. Morsony³, and Jared C. Workman⁴

¹ *Department of Physics, 301 Weniger Hall, Oregon State University, Corvallis, OR 97331*

² *Reed College, 3203 Southeast Woodstock Boulevard Portland, Oregon 97202-8199*

³ *Department of Astronomy, University of Maryland, 1113 Physical Sciences Complex, College Park, MD 20742-2421, USA*

⁴ *Department of Physical and Environmental Sciences, Colorado Mesa University, Grand Junction, CO 81501, USA*

3 July 2017

ABSTRACT

We present calculations of the wide angle emission of short-duration gamma-ray bursts from compact binary merger progenitors. Such events are expected to be localized by their gravitational wave emission, fairly irrespective of the orientation of the angular momentum vector of the system, along which the gamma-ray burst outflow is expected to propagate. We show that both the prompt and afterglow emission are dim and challenging to detect for observers lying outside of the cone within which the relativistic outflow is propagating. If the jet initially propagates through a baryon contaminated region surrounding the merger site, however, a hot cocoon forms around it. The cocoon subsequently expands quasi-isotropically producing its own prompt emission and external shock powered afterglow. We show that the cocoon prompt emission is detectable by Swift BAT and Fermi GBM. We also show that the cocoon afterglow peaks a few hours to a few days after the burst and is detectable for up to a few weeks at all wavelengths. The timing and brightness of the transient are however uncertain due to their dependence on unknown quantities such as the density of the ambient medium surrounding the merger site, the cocoon energy, and the cocoon Lorentz factor. For a significant fraction of the gravitationally-detected neutron-star-binary mergers, the cocoon afterglow could possibly be the only identifiable electromagnetic counterpart, at least at radio and X-ray frequencies.

Key words: gamma-ray burst: general – radiation mechanisms: non-thermal – gravitational waves

1 INTRODUCTION

Short duration gamma-ray bursts (SGRBs) are expected to be associated with the merger of a compact binary system in which at least one of the two components is a neutron star (NS), the other possibly being a black hole (BH; Eichler et al. 1989; Nakar 2007; Berger 2014). Binary NS¹ mergers are also candidate sources of gravitational waves, similar to the binary BH mergers recently detected by LIGO (Phinney 1991; Shibata & Uryū 2002; Faber & Rasio 2002; Sekiguchi et al. 2011; Abbott et al. 2016a,b). While a SGRB is highly beamed and its detection against the gamma-ray background is possible only if its relativistic jet is pointing towards the Earth, gravitational waves are only mod-

erately aspherical and NS binary mergers are expected to be detectable irrespective of their orientation. For a typical SGRB jet opening angle of 16° (Fong et al. 2015), the probability of detecting an on-axis burst is only ~ 10 per cent². In other words, only one out of 10 NS binary mergers detected in gravitational waves (GWs) will be accompanied by a full-fledged SGRB. Other estimates put the average opening angle at $\sim 6^\circ$ (Ghirlanda et al. 2016), with a rate of only one on-axis burst every ~ 100 detected by LIGO. The most likely orientation will be the one most difficult to observe in electromagnetic waves, i.e., the edge-on configuration with the relativistic jet expanding perpendicularly to the line of sight. Our hope of confirming the supposed association of

¹ Here and in the following we call binary NS a system in which at least one of the components is a NS, the other being either a NS or a BH.

² Here and in the following, these estimates include the angle dependency of the GW strain, which is larger for a face-on binary system, likely producing an on-axis burst (Abadie et al. 2012)

SGRBs with NS binary mergers (Shibata & Taniguchi 2006; Faber et al. 2006; Giacomazzo et al. 2013; Fong & Berger 2013; Ruiz et al. 2016) is therefore tied to our capability of modeling and detecting the off-axis emission of such events (Metzger & Berger 2012). While said emission is faint, compared to the burst of gamma rays from an on-axis jet, LIGO only detects NS binary mergers within a relatively small distance from Earth (~ 200 Mpc), and even the faint off-axis SGRB components might be detectable.

Off-axis emission from relativistic jets in the external shock phase has been studied for long and short duration GRBs, especially for the late afterglow phase (Rhoads 1999; Granot et al. 2002; Rossi et al. 2004; Rossi, Perna, & Daigne 2008; van Eerten, Zhang, & MacFadyen 2010; Salafia et al. 2015, 2016). While such off-axis events have been searched in multi-wavelength surveys, no credible candidate has emerged, so far (Greiner et al. 2000; Nakar, Piran, & Granot 2002; Rau & Greiner 2005; Rykoff et al. 2005; Rau, Greiner, & Schwarz 2006; Guidorzi et al. 2009; Ghirlanda et al. 2015). The case of GW-detected NS binary mergers would, however, be different. If a localization could be made for the direction to the GW event, searching for a transient in a small area of the sky would be much easier than blindly surveying a large region of the sky. Detection of off-axis emission from SGRBs associated with gravitationally detected binary NS mergers could then become a powerful tool for studying the structure of the jet and of any non-relativistic or mildly relativistic ejecta associated with the merger and the burst.

In light of these considerations, we present in this paper a calculation of possible components of off-axis emission from a SGRB, including the de-beamed prompt emission, the emission associated with the jet cocoon (Ramirez-Ruiz, Celotti, & Rees (2002); Nakar & Piran (2017) who, however, considered mainly the cocoons of long duration GRBs), and the afterglow emission. This paper is organized as follows: in Section 2 we present the theoretical framework at the base of our calculations, in Section 3 we present our multi-wavelength results, and in Section 4 we discuss the detectability of the signal for expected distances of LIGO-detected NS binary mergers and the implications of a (non)detection.

2 EMISSION COMPONENTS

We consider a SGRB engine releasing a total energy E_2 in two counter-propagating jets. $E_1 = E_2/2$ is the energy released in each jet. The engine is active for a time t_{eng} and the outflow is initially beamed in jets with an half-opening angle θ_j . The jets are released at rest ($\Gamma_0 = 1$) at a distance r_0 from the center of the system with a ratio of internal energy to rest mass allowing for acceleration to a maximum Lorentz factor Γ_∞ . The isotropic equivalent energy of the system is $E_{\text{iso}} = 4\pi E_2/\Omega_2$, where $\Omega_2 = 4\pi(1 - \cos\theta_j)$ is the solid angle occupied by the two jets. The rest mass carried by the fireball is $m_0 = E_2/\Gamma_0 c^2$. We consider to counter-propagating “top-hat” jets, with uniform properties within their opening angle θ_j and with sharp edges.

Guided by binary merger simulation results (Kiuchi et al. 2014, 2015; Radice et al. 2016) we assume that the jet is launched and initially propagates within a baryon contam-

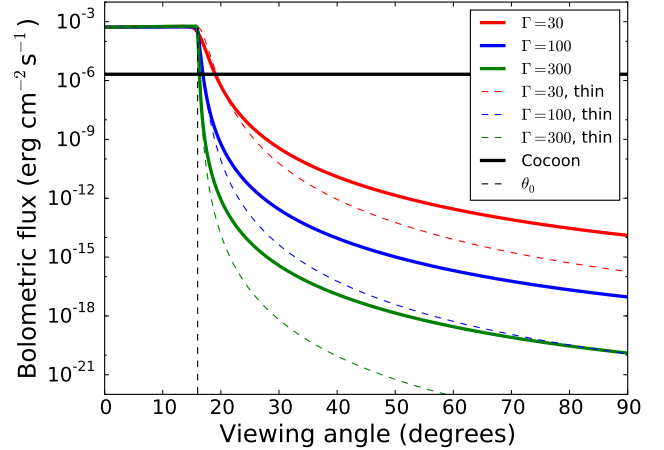


Figure 1. Bolometric peak flux of the prompt emission of a short GRB as a function of the observer viewing angle. The burst characteristics are from the fiducial values in Table 1 and is located at a distance of 200 Mpc from Earth. Three values of the Lorentz factor are shown, as well as the isotropic cocoon contribution. The thin dashed line shows the result for a radially thin outflow that emits for a vanishingly small time.

inated environment. We assume the polluted region to be of size R_a and to have uniform density ρ_a . Due to the very short interaction time with the expanding jet, we neglect any expansion of the polluted region, which is predicted to be moving outward at non-relativistic (NR) speed.

2.1 Prompt emission

The prompt emission of the SGRB jet is computed as follows (see also Yamazaki, Ioka, & Nakamura (2002, 2003); Yamazaki, Yonetoku, & Nakamura (2003) for analogous calculations for long GRBs). We assume that at a certain distance R_{rad} from the engine the internal energy of the outflow is converted into photons and radiated. The nature of the emission mechanism is not discussed here and is irrelevant for our conclusions. We assume that there are no small-scale relativistic internal motions such as those predicted by turbulence-driven models (Narayan & Kumar 2009) and some magnetic reconnection models (Zhang & Yan 2011). We also assume that the local dissipation rate in the outflow comoving frame is uniform within the jet opening angle and that the emitted radiation is isotropic in the local comoving frame.

We first consider the peak bolometric luminosity $L_{\text{prompt,pk}}$, so that the details of the spectral shape of the prompt emission do not need to be discussed. Its variation for observers along different lines of sight depends on the timing properties of the jet emission. We first consider the case in which the duration of the emission episode in the comoving frame is long enough that every observer sees emission from the entire outflow, at least at some time. Under such conditions, the received bolometric flux is the result of the integration over the emitting surface of the local emission boosted by the Doppler factor $\delta(\Gamma, \theta) = [\Gamma(1 - \beta \cos\theta)]^{-1}$ elevated to the fourth power (one for the photon rate, one for the blueshift in the photon energy, and two for the beaming

Table 1. List of symbols used and their meaning. Fiducial values are given for primary quantities. Variables for which a fiducial value is not reported can be derived from the primary ones. The calculated fluxes at one day for the on-axis SGRB with our fiducial properties, for a source at $z = 0.5$, are $f_{\text{keV}} = 0.05 \mu\text{Jy}$; $R_{AB} = 22$, and $f_{8\text{GHz}} = 100 \mu\text{Jy}$. All these fluxes are within the distributions of the observed values as reported in Figure 1 of Fong et al. (2015), making our fiducial values adequate. The optical magnitude is in the brighter end of the observed distribution, and our optical band estimates may therefore be slightly optimistic (see also Figure 2 of Li et al. 2016).

Symbol	Fiducial value	Meaning
E_2	2×10^{50} erg	Total energy released by the engine in two jets
E_1		Total energy released by the engine in one jet
L_2		Engine luminosity in two jets
E_{iso}		Isotropic equivalent energy released by the engine
t_{eng}	1 s	Time during which the engine is active
θ_j	16°	Half-opening angle of each jet
Ω_2		Solid angle occupied by the two jets
Γ_0	1	Lorentz factor of the jet at the injection radius r_0
Γ_∞	100	Maximum Lorentz factor the jet can attain
m_0		Rest mass of the outflow
r_0	10^7 cm	Radius at which the jet is launched
θ_{obs}		Angle between the jet axis and the line of sight
$\theta_{v,\text{obs}}$		Angle between the line of sight and the velocity vector of an outflow element
θ_v		Angle between the velocity vector of an outflow element and the jet axis
β_h		Velocity of the head of the jet in units of the speed of light
β_j		Velocity of the jet material in units of the speed of light
R_a	10^8 cm	Radius of the sphere polluted by NR ejecta
ρ_a	10^7 g/cm ³	Density of the sphere polluted by NR ejecta
R_{rad}	10^{13} cm	Radius at which the fireball begins releasing the prompt emission photons
$L_{\text{prompt,pk}}$		Peak bolometric luminosity of the prompt emission
Σ		Emitting surface of the SGRB outflow
δ		Doppler factor
α_{ph}	0	Low-frequency photon index of the prompt Band spectrum
β_{ph}	-2.5	High-frequency photon index of the prompt Band spectrum
$h\nu'_{\text{pk}}$	2.5 keV	Comoving peak photon energy of the prompt Band spectrum
ϵ_e	0.1	Fraction of the external shock energy in non-thermal electrons
ϵ_B	0.01	Fraction of the external shock energy in magnetic field
n_{ISM}	0.1 cm^{-3}	density of the ambient medium for the afterglow calculations
p	2.5	Index of the non-thermal electron energy distribution ($p(\gamma) \propto \gamma^{-p}$)
$\delta t'_{\text{rad}}$	200 s	Comoving duration of the prompt emission
t_{bo}		Breakout time of the jet off the ambient material
E_c	10^{49} erg	Cocoon energy
L_c		Prompt emission luminosity of the cocoon
Σ_j		Cross-sectional area of the two jets at break-out
$\Gamma_{\infty,c}$	10	Asymptotic Lorentz factor of the cocoon material
$R_{\text{sat},c}$		Saturation radius of the cocoon
$R_{\text{ph},c}$		Photospheric radius of the cocoon
$T_{0,c}$		Initial temperature of the cocoon at breakout time
$T_{\text{ph},c}$	10 keV	Observed photospheric temperature of the cocoon
V_c		Volume of the cocoon at breakout time
δt_{diff}		Photon diffusion time in the outflow at the photosphere
δt_{ang}		Angular timescale of the fireball at the photosphere

of the solid angle). The observed peak bolometric luminosity is therefore calculated as:

$$L_{\text{prompt,pk}}(\theta_{\text{obs}}) = L_{\text{prompt,pk}}(0) \frac{\int_{\Sigma} \delta^4(\Gamma_0, \theta_{v,\text{obs}}) d\sigma}{\int_{\Sigma} \delta^4(\Gamma_0, \theta_v) d\sigma} \quad (1)$$

where θ_{obs} is the angle between the line of sight and the jet axis that points nearest to the observer, Σ is the emitting surface, $\theta_{v,\text{obs}}$ is the angle between the line of sight and the local velocity vector, θ_v is the angle between the local velocity vector and the jet axis, and $L_{\text{prompt,pk}}(0)$ is the peak luminosity seen by an on-axis observer. The results of the above integration for various values of Γ_0 are shown in Figure 1. The main lesson from the figure is that, for expected values of the fireball Lorentz factor at the time of the prompt

emission, the observed flux drops-off quite dramatically as soon as the line of sight moves out of the jet.

We note that the assumptions above are quite optimistic. Let us consider now the opposite assumption, i.e., a jet in which the emission lasts for a negligibly small amount of time in the comoving frame. In this case each observer sees only a small region of the jet active at any time, and the peak flux is due solely to the region of the fireball closer

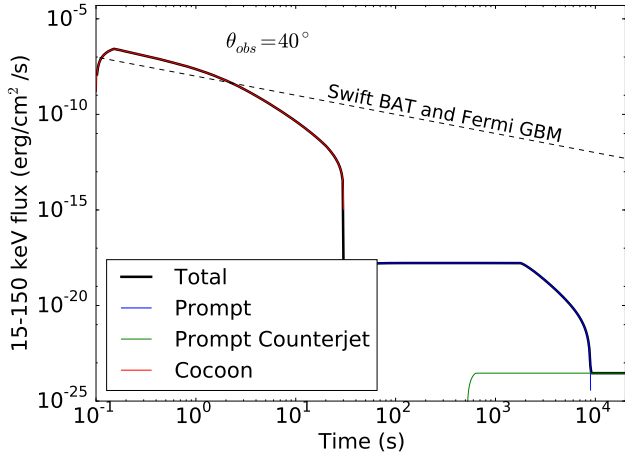


Figure 2. Prompt emission from a short GRB seen at 40° off-axis in the Swift BAT or Fermi-GBM bands. The thresholds of the two instruments, which are similar for a low-temperature thermal source, are shown for comparison.

to the line of sight. Eq. 1 is replaced by the simpler:

$$L_{\text{prompt,pk}}(\theta_{\text{obs}}) = L_{\text{prompt,pk}}(0) \frac{\delta^4(\Gamma_0, \theta_{v,\text{obs,min}})}{\delta^4(\Gamma_0, \theta_v)}$$

$$\sim \begin{cases} L_{\text{prompt,pk}}(0) & \theta_{\text{obs}} \leq \theta_j \\ \frac{L_{\text{prompt,pk}}(0)}{16\Gamma_0^8 [1 - \beta \cos(\theta_{\text{obs}} - \theta_j)]^4} & \theta_{\text{obs}} > \theta_j \end{cases} \quad (2)$$

which decays even faster than the one from Equation 1 for large off-axis angles (see dashed lines in Figure 1).

For the calculation of the light curves in the radio, optical, X-ray, and Swift BAT band, instead, we proceeded as follows. We assumed that the prompt emission has a Band spectral shape with $\alpha_{\text{ph}} = 0$, $\beta_{\text{ph}} = -2.5$, and comoving peak frequency $h\nu'_{\text{pk}} = 2.5$ keV. We also assumed that the emission of radiation turns on at the same radius R_{rad} for the entire fireball and lasts, in the comoving frame $\delta t'_{\text{rad}} = 200$ s. As seen from an on-axis observer ($\theta_{\text{obs}} = 0$) and assuming $\Gamma_\infty = 100$, this burst has an observed peak photon energy $h\nu_{\text{pk}} \sim 500$ keV and a duration $\delta t_{\text{rad}} \sim 1$ s, fairly typical for observed SGRBs. The spectrum was normalized such that the on-axis observer would detect a bolometric isotropic equivalent energy 2.5×10^{51} erg, corresponding to a prompt emission efficiency of 50 per cent.

The prompt emission light curves in Figures 2, 3, 4, and 5 were computed via a Monte Carlo method. Three million emission regions were generated with random propagation direction within the jet opening angle. Each of them was turned on at the prescribed distance and given the Band spectrum described above. The observed activation time of each emission region was calculated taking into account light propagation effects, and the observed light curve of each individual region was calculated by integrating the Band spectrum in the comoving frequency band corresponding to the observed frequency range. All the emission regions were then coadded in the final light curves.

2.2 Cocoon emission

2.2.1 Cocoon energy

We derive the energy that is transferred from the jet into the cocoon under the assumption that the jet head travels at a constant velocity. This allows us to write the energy of the cocoon as the luminosity of two jets, $L_2 = E_2/t_{\text{eng}}$ times the amount of time the jets spend in the ambient material, t_{bo} : $E_c = L_2 t_{\text{bo}}$. We can express t_{bo} as the distance the jet has to travel, R_a , divided by the velocity of the jet head, β_h , giving:

$$E_c = \frac{L_2 R_a}{c \beta_h}, \quad (3)$$

which leaves the head velocity, β_h , as the only quantity to derive. We consider two methods for deriving β_h . The first (Morsony, Lazzati, & Begelman 2007; Bromberg et al. 2011) assumes that the jet transversal size is obtained by equating the ram pressure of the jet material with the pressure of the cocoon. This method should therefore be appropriate for cocoon-confined jets, those for which the outflow velocity vector makes a significant angle with the jet-cocoon discontinuity. They first define the quantity (see also Matzner 2003):

$$\tilde{L} = \frac{L_2}{\Sigma_j \rho_a c^3}, \quad (4)$$

the ratio between the energy density of the jet and the energy density of the surrounding medium, where L_2 is the luminosity of the two jets and $\Sigma_j = R_a^2 \Omega_2$ is the cross-sectional area of the jet at breakout. By making cylindrical approximations for the jet, they show it is approximately

$$\tilde{L} \simeq \left(\frac{L_2 \pi^2}{\rho_a t_{\text{bo}}^2 \Omega_2^2 c^5} \right)^{2/5}. \quad (5)$$

Then, following Matzner (2003), we find

$$\beta_h = \frac{\beta_j}{1 + \tilde{L}^{-1/2}}, \quad (6)$$

For the values considered in this paper (see Table 1), $\tilde{L} \ll 1$ and therefore

$$\beta_h \simeq \tilde{L}^{1/2}. \quad (7)$$

Therefore, with $t_{\text{bo}} = R_a/c\beta_h$, the energy in the cocoon is

$$E_c = \left(L_2^2 R_a^5 \rho_a \Omega_2^2 \pi^{-2} \right)^{1/3}. \quad (8)$$

Using the values presented in Table 1, this gives an energy of $E_c = 4.2 \times 10^{48}$ erg.

An alternative derivation of β_h can be obtained by balancing the jet thermal pressure and the cocoon pressure to compute the jet transversal size (Lazzati & Begelman 2005; Lazzati et al. 2012). This approximation holds for mildly confined jets, for which the ram pressure is negligible due to the fact that the relativistic outflow velocity is nearly parallel to the jet-cocoon discontinuity. They find:

$$\beta_h = \left(\frac{2L_2^3}{\pi c^9 r_0^4 R_a^2 \Omega_2^2 \rho_a^3} \right)^{1/7}, \quad (9)$$

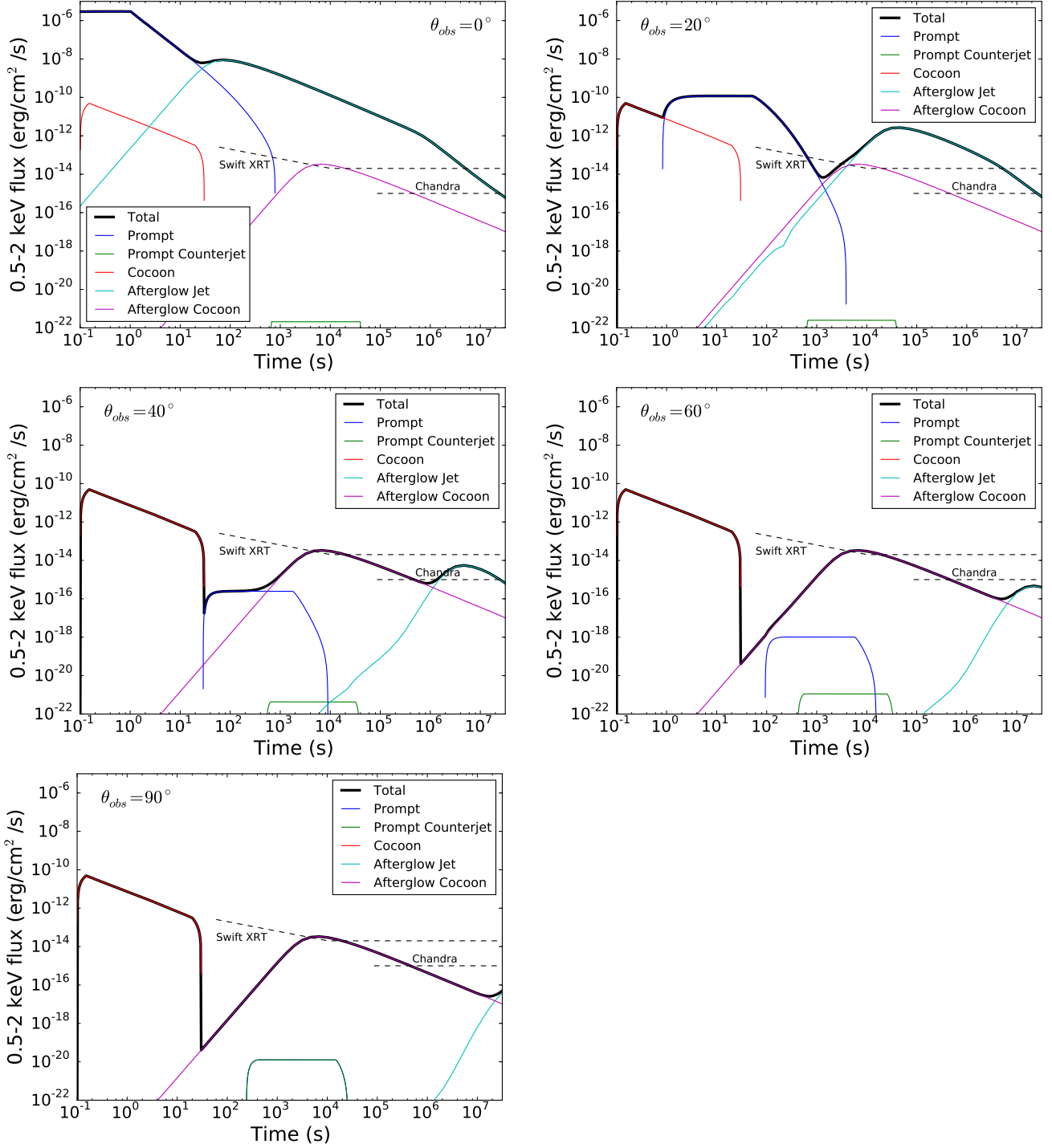


Figure 3. X-ray light curves from a SGRB at 200 Mpc. Each panel shows the various components (thin colored lines) and the total (solid black) flux for a unique observer. Observers are located at 0, 20, 40, 60, and 90° from the jet axis, respectively.

which gives a cocoon energy:

$$E_c = \left(\frac{L_2^4 R_a^9 t_0^4 \Omega_2^2 \rho_a^3 c^2 \pi}{2} \right)^{1/7}, \quad (10)$$

which gives an energy of $E_c \simeq 7 \times 10^{48}$ erg for the fiducial values reported in Table 1.

The two results for the cocoon energy are fairly similar. Not surprisingly, the second value gives a higher cocoon en-

ergy, since the jets are only mildly confined by the relatively low density of the merger ejecta. In the following we adopt a fiducial value $E_c = 10^{49}$ erg for the cocoon energy. We note that the cocoon energy depends less than linearly on all jet and ejecta properties with the exception of the radius of the polluted region. Should the ejecta be distributed in a larger region than the one assumed here, the cocoon energy would be significantly higher. To test the dependency of

the detectability of the cocoon on the uncertain energetics, we subsequently test values of the cocoon energy ten times lower and higher than our fiducial value.

2.2.2 Cocoon dynamics and radiation

Let us now consider the subsequent evolution of the cocoon. At breakout, the cocoon is hot and high-pressured with no associated bulk motion. Upon release, it accelerates quasi-isotropically (Ramirez-Ruiz, Celotti, & Rees 2002; Nakar & Piran 2017). The light curve produced by the cocoon depends critically on the contamination from the ambient material. Numerical simulations of long GRB jets show that the cocoon is polluted by the progenitor material in such a way that it has an asymptotic Lorentz factor $\Gamma_{\infty,c} \sim 10$ (Lazzati, Morsony, & Begelman 2010). We therefore adopt a value $\Gamma_{\infty,c} = 10$ in the remainder of this study, but we warn the reader that dedicated numerical simulations should be performed to pin down the actual composition of SGRB cocoons (see, e.g., Gottlieb, Nakar, & Piran (2017)).

Initially, the cocoon fireball accelerates self similarly, $\Gamma \propto r$, until the saturation radius (e.g., Cavallo & Rees 1978; Chhotray & Lazzati 2017):

$$R_{\text{sat},c} = \Gamma_{\infty,c} R_a \quad (11)$$

Beyond the saturation radius the cocoon fireball coasts at constant Lorentz factor, releasing the advected radiation at the photospheric radius (Mészáros & Rees 2000):

$$R_{\text{ph},c} = \left(\frac{E_c \sigma_T}{8\pi m_p \Gamma_{\infty,c}^3 c^2} \right)^{\frac{1}{2}} \quad (12)$$

which is, for the parameter choices of Table 1, beyond the saturation radius $R_{\text{sat},c}$. The observed cocoon temperature is constant during the acceleration phase, and scales as $r^{-2/3}$ in the coasting phase, yielding a photospheric temperature:

$$T_{\text{ph},c} = T_{0,c} \left(\frac{R_{\text{ph},c}}{R_{\text{sat},c}} \right)^{-\frac{2}{3}} = \left(\frac{E_c}{aV_c} \right)^{\frac{1}{4}} \left(\frac{E_c \sigma_T}{8\pi m_p R_a^2 \Gamma_{\infty,c}^5 c^2} \right)^{-\frac{1}{3}} \quad (13)$$

where $T_{0,c} = (E_c/aV_c)^{1/4}$ is the initial temperature of the cocoon, a is the radiation constant and V_c is the cocoon volume at breakout time. Following Lazzati & Begelman (2005) we find:

$$V_c = \frac{2}{3\beta_{\text{h},c}} \sqrt{\frac{\pi E_c R_a^3}{\rho_a}} \quad (14)$$

yielding an observed cocoon photospheric temperature:

$$T_{\text{ph},c} = \left(\frac{24}{a} \right)^{\frac{1}{4}} \pi^{\frac{5}{24}} c^{\frac{11}{12}} \left(\frac{m_p}{\sigma_T} \right)^{\frac{1}{3}} \frac{\beta_{\text{h},c}^{\frac{1}{4}} \rho_a^{\frac{1}{8}} \Gamma_{\infty,c}^{\frac{5}{3}} R_a^{\frac{7}{24}}}{E_c^{\frac{5}{24}}} \quad (15)$$

Adopting the fiducial SGRB values from Table 1 and the jet head velocity from either Equation 7 or 9 we find $T_{\text{ph},c} \approx 10$ keV, the value that we adopt for the light curves calculations.

Assuming that the radiated spectrum is a black body³

³ In the absence of internal dissipation and magnetic fields, the spectrum is expected to be a broadened black body (Goodman 1986; Lazzati 2016; De Colle et al. 2017).

we obtain a luminosity:

$$L_c = \sigma \pi \left(\frac{R_{\text{ph},c}}{\Gamma_{\infty,c}} \right)^2 T_{\text{ph},c}^4 = \frac{3m_p^{\frac{1}{3}} \pi^{\frac{5}{6}} \sigma c^{\frac{5}{3}}}{\sigma_T^{\frac{1}{3}} a} E_c^{\frac{1}{6}} \Gamma_{\infty,c}^{\frac{5}{3}} \beta_{\text{h},c}^{\frac{1}{3}} \rho_a^{\frac{7}{6}} R_a^{\frac{7}{6}} \quad (16)$$

where we have used Equations 12 and 13 for the final result. For the typical SGRB values adopted above, we have:

$$L_c = 4 \times 10^{49} \left(\frac{E_c}{10^{49}} \right)^{\frac{2}{3}} \left(\frac{\Gamma_{\infty,c}}{10} \right)^{\frac{5}{3}} \left(\frac{R_a}{10^8} \right)^{-\frac{1}{3}} \quad (17)$$

The emission would last for the longest time between the diffusion time in the cocoon shell $\delta t_{\text{diff}} \sim R_a/c$ and the angular time scale $\delta t_{\text{ang}} = R_{\text{ph},c}/(c\Gamma_{\infty,c}^2)$. For $\Gamma_{\infty,c} = 10$ the latter dominates and the cocoon thermal pulse would last ~ 0.3 s. Note that multiplying the photospheric luminosity times the pulse duration we obtain a photospheric radiative energy that is comparable (within a factor of order unity) to the cocoon energy, as expected.

The light curves of the cocoon photospheric emission shown in Figures 2, 3, 4, and 5 were computed via the same Monte Carlo method discussed for the prompt emission. The comoving spectrum, however, was assumed to be thermal with temperature $T'_{\text{ph},c} = 1$ keV.

2.3 Afterglow

The afterglow emission of the jet and cocoon components are calculated using the semi-analytic Trans-Relativistic Afterglow Code (TRAC), identical to that used in Morsony, Workman, & Ryan (2016) (full description will be published in Morsony et al. in preparation). TRAC is able to model the emission of a relativistic fireball with an arbitrary energy distribution, as seen by an observer at any angle relative to the jet axis. We assume all afterglow emission is produced by synchrotron radiation, including synchrotron self-absorption and local synchrotron cooling. For all models presented here, synchrotron radiation is parameterized by $\epsilon_e = 0.1$, the fraction of energy in electrons, $\epsilon_B = 0.01$, the fraction of energy in the magnetic field, and $p = 2.5$, the spectral index of the electron energy distribution.

We model the jet and cocoon as expanding into a constant density external medium (ISM) with number density of $n_{\text{ISM}} = 10^{-1} \text{ cm}^{-3}$. The cocoon component is modeled as a spherical explosion with kinetic energy of $E_c = 10^{49}$ erg and initial Lorentz factor of $\Gamma_{\infty,c} = 10$. The jet is modeled as a top-hat jet with isotropic-equivalent kinetic energy of $E_{\text{iso}} = 2.5 \times 10^{51}$ erg (half of the initial energy, since 50 per cent of it was released as gamma-ray radiation in the prompt emission) and initial Lorentz factor $\Gamma_{\infty} = 100$ within an half opening angle $\theta_j = 16^\circ$ and no material outside the jet.

3 RESULTS

Figures 2, 3, 4, and 5 summarize the results of our calculations. Figure 2 shows how the prompt emission of an off-axis SGRB would be seen by wide field X-ray and γ -ray monitors on board Swift and Fermi.

The three other figures show how a burst with the properties listed in Table 1 and located at 200 Mpc from Earth would be observed in X-rays, optical, and radio bands, respectively. Each figure has five panels, each panel showing

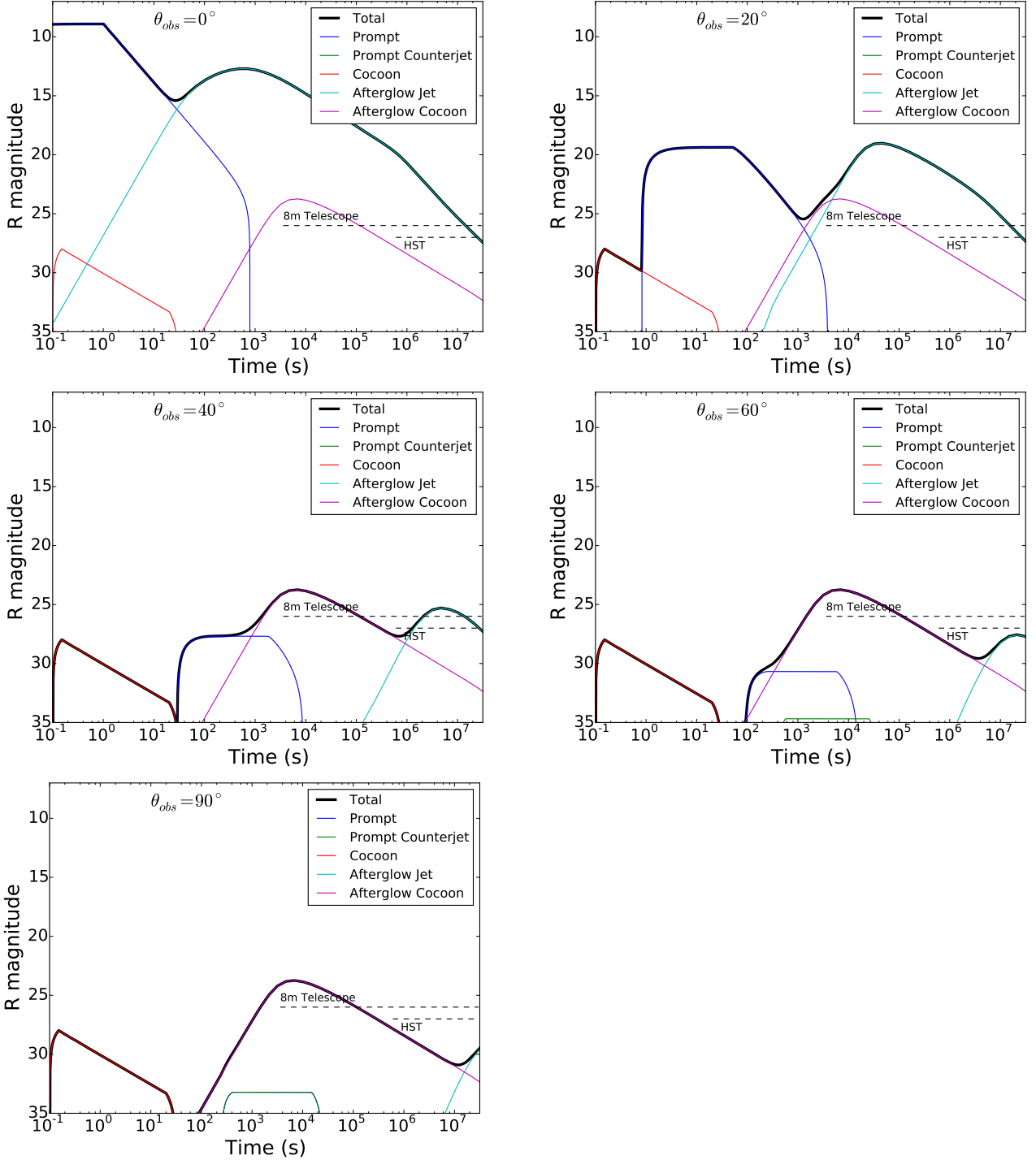


Figure 4. Same as Figure 3 but showing R-band magnitudes.

the observations that would be performed by an observer located along a particular line of sight. From left to right and top to bottom, observers at 0, 20, 40, 60, and 90 degrees from the jet axis are shown. Along with the predicted fluxes and flux densities, we show the detection limit of instruments that could be used to search for the electromagnetic counterpart of the GW event. In X-ray, we consider Swift XRT and Chandra. For late XRT observations we assume a detection limit of 2×10^{-14} erg cm $^{-2}$ s $^{-1}$ (for a 10 ks exposure). For

early XRT observations, we assume a detection limit that scales with the square root of the exposure time, assuming that the signal to noise is background dominated. A constant detection limit of 10^{-15} erg cm $^{-2}$ s $^{-1}$ is adopted for Chandra, corresponding to a ~ 50 ks exposure. We also assumed that Swift can repoint XRT to the burst location within one minute, while it takes Chandra one day to repoint. In the optical we show R-band imaging detection limits for an 8 meter class telescope and for HST, R=26 and 27, respec-

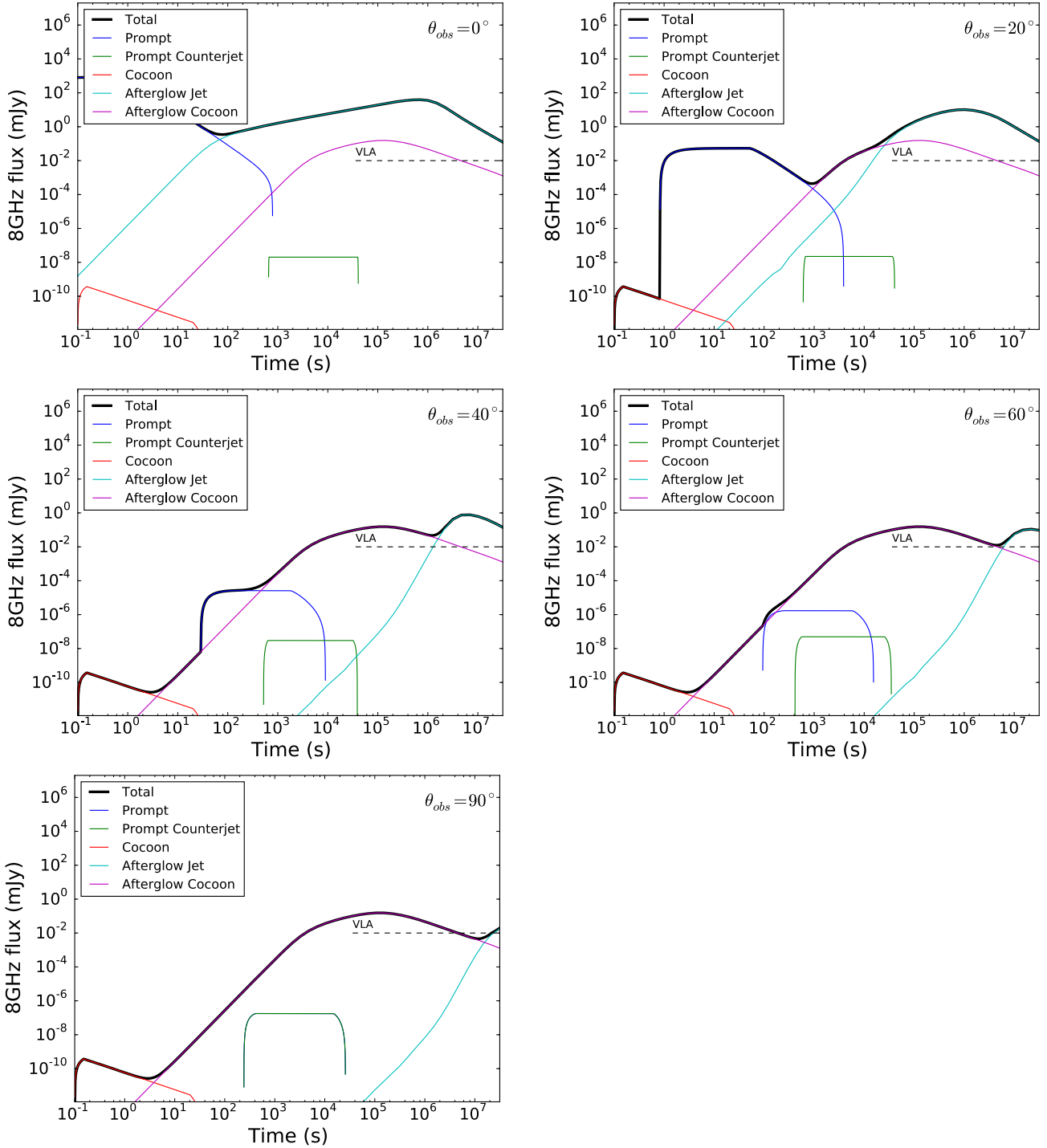


Figure 5. Same as Figure 3 but showing 8 GHz flux densities.

tively. Finally, in the radio, we report a VLA detection limit of $10 \mu\text{Jy}$, assuming a 10 hours reaction time.

Due to the unknown nature of the cocoon energy E_c , its Lorentz factor $\Gamma_{\infty,c}$, its geometry, and the equipartition parameters of the external shock ϵ_e and ϵ_B , and the interstellar density n_{ISM} , we have explored cocoon afterglows for a range of all those parameters. In particular, we explore afterglows from cocoon with $E_c = 10^{48}$, 10^{49} , and 10^{50} erg; Lorentz factor $\Gamma_{\infty,c} = 2$, 5, and 10; $\epsilon_e = 0.01$, 0.03, and 0.1; $\epsilon_B = 10^{-4}$,

10^{-3} , and 10^{-2} ; and $n_{\text{ISM}} = 0.001$, 0.01, and 0.1 cm^{-3} . For each combinations of the above parameters, the X-ray, optical, and radio afterglow are computed. The peak fluxes for the three bands are shown in Figure 6 versus the time of the peak. It is obvious that the uncertainty in the cocoon physics and external shock properties cause significant spread in the prediction. The brightest transients, however, always peak a few hours after the burst in the X-ray and optical, and within \sim a week in the radio.

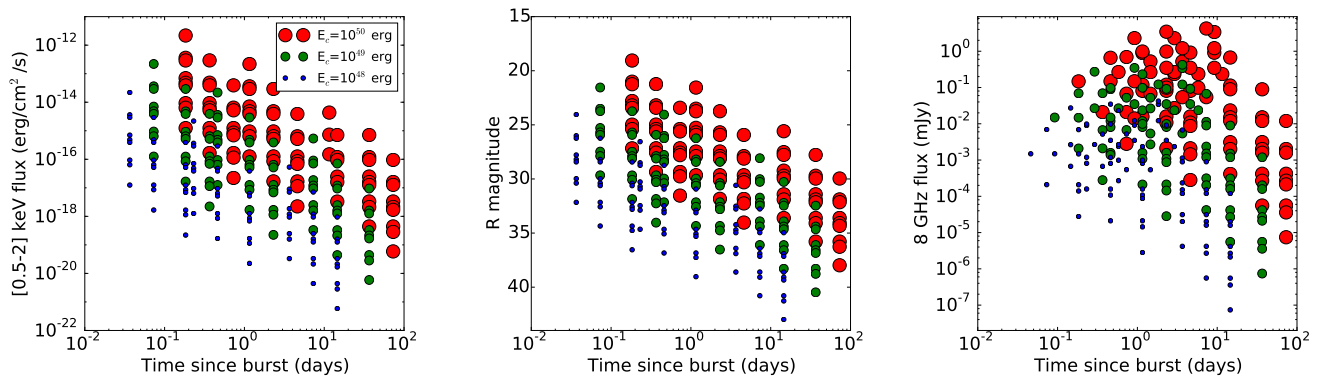


Figure 6. Peak emission fluxes vs. peak times for cocoon afterglows from a range of cocoon and external shock properties (see text). The unknown cocoon physics and properties of the external shock cause a significant uncertainty on the detectability of the EM transient from off-axis observers.

4 SUMMARY AND DISCUSSION

We have calculated the on- and off-axis emission of a typical short GRB. Our calculations include the prompt and afterglow emission from the relativistic jet material as well as the prompt and afterglow emission from the cocoon material. An energetic cocoon is expected to form as the SGRB relativistic jet propagates through the immediate surroundings of the NS binary merger, polluted with $\sim 0.01 M_{\odot}$ of material tidally ejected from the merging compact objects (Kiuchi et al. 2014, 2015; Radice et al. 2016). We calculated the energy of the cocoon and find it to amount to approximately 10 per cent of the burst energy and to be a strong function of the size of the high-density region surrounding the merger site.

As reported in Figures 3, 4, and 5, the emission from the relativistic jet (both prompt and afterglow) dominate at all times and at all wavelengths for the on-axis observer. However, as discussed above, the most likely observer angles are large, half of the events been observed at 35 degrees or more. In such cases (Figure 2 and the last three panels of Figures 3, 4, and 5) the jet emission is undetectable with current instrumentation, with the exception of the radio band, in which a $100 \mu\text{Jy}$ source would be detectable approximately one year after the GW detection. A faint optical transient peaking ~ 2 months after the GW trigger would also be detectable for observers at $\theta_{\text{obs}} < 50^{\circ}$. This is due to the fact that the emission from an off-axis jet is dramatically reduced by relativistic beaming (see Figure 1), and the jet emission is detected only after the jet has slowed down to trans-relativistic speed, about one year after the merger. The cocoon afterglow, instead, is isotropic and peaks at a few hours (X-rays and optical) to a few days (radio) after the merger. At peak time, and for a few days to a few weeks, it is faint but clearly detectable by current instrumentation. However, the faint multiwavelength afterglow would require previous localization in order to be observable with narrow-field instruments. The faint but detectable X-ray thermal pulse of the prompt cocoon emission gives therefore the best hope of localizing the EM counterpart of a GW-detected binary NS merger (see Figure 2).

We therefore conclude that, should a GW detected NS binary merger be promptly localized, rapid follow up would

be able to detect the cocoon afterglow emission and allow for the identification of the electromagnetic counterpart of the GW source. Besides being brighter, the cocoon emission is detectable just a few hours after the GW signal, greatly reducing the likelihood of a false detection triggered by an unrelated transient within the error radius of the GW source. The cocoon also produces a short (~ 0.3 s) pulse of prompt emission with a broadened thermal spectrum. According to our calculations, the cocoon prompt emission is just above the detection threshold of both the Swift BAT and the Fermi GBM.

Our calculations are based on a set of simplifying assumptions. First, we assume that the relativistic outflow is a top-hat jet, with a sharp edge in which the Lorentz factor drops from 100 to 1 with no boundary layer. The jet is assumed not to spread laterally. However, sideways expansion does not change significantly the afterglow luminosity, even for off-axis observers (compare Figures 6 and 7 of Rossi et al. (2004)). We also assume that the cocoon is perfectly isotropic, and that some degree of mixing with the ambient medium causes the entropy of the cocoon to be lower than the one of the jet material. While these assumption allow us to perform the calculations using semi-analytical techniques, they might overemphasize the differences between the on-axis and off-axis observers (see, e.g., the results of the simulations of Gottlieb, Nakar, & Piran (2017)). For example, a jet with a transition layer with lower Lorentz factor would produce a smoother decline of the prompt emission with observer angle (compared to the dramatic decrease seen in Figure 1). In addition, a cocoon that maintains some degree of asymmetry would be dimmer – and therefore harder to detect – for a binary merger with a very large viewing angle. In Figure 6 we show the consequence of changing the values of our fiducial parameters on the afterglow fluxes in the X-ray, optical, and radio bands. Finally, we neglect the effect of X-ray scattering that could add a quasi-isotropic component to the SGRB emission (Kisaka, Ioka, & Nakamura 2015).

Numerical simulations need to be performed to correctly represent the ambient medium and self-consistently predict the jet structure and the cocoon structure and degree of mixing with the ambient medium. We also should note that we neglect the emission from a kilonova (also known as

a macronova), possibly associated with the merger (Li & Paczyński 1998; Metzger et al. 2010; Kasen, Fernández, & Metzger 2015; Kisaka, Ioka, & Takami 2015). The kilonova emission is isotropic and should be sufficiently bright in the optical and IR bands ($R \sim 24$ at 200 Mpc) and peak at ~ 1 week after the merger. It would therefore be identified easily from the cocoon and jet afterglows that peak on time scales of a few hours and a few months (for a large angle observer). A kilonova precursor peaking ~ 1 hour after the merger has also been discussed (Metzger et al. 2015), possibly outshining the cocoon optical afterglow component at early time.

To conclude, we would like to point out the opportunity given by the follow-up of GW detected binary merger to pin down the jet structure of SGRBs. When a large sample of GW detected NS binary mergers will be available, comparing the brightness of their electromagnetic counterparts could allow us to map the polar distribution of the jet energy, velocity, and possibly magnetization. This would be an extremely important constrain for jet acceleration models that is impossible to obtain from long-duration GRBs. However, no GW emission from binary NS mergers has been detected so far, and using multimessenger detections for constraining jet parameters may be a feat that will be possible only many decades from today.

ACKNOWLEDGEMENTS

We thank Giancarlo Ghirlanda, Edo Berger, and Brian Metzger for useful discussions. DL acknowledges support from NASA ATP grant NNX17AK42G. AD thanks the department of Physics of Oregon State University for the hospitality during part of the preparation of this paper. BJM was supported by the NSF under grant AST-1333514 and by the Aspen Center for Physics under NSF grant PHY-1066293

REFERENCES

- Abadie J., et al., 2012, ApJ, 760, 12
 Abbott B. P., et al., 2016, PhRvL, 116, 061102
 Abbott B. P., et al., 2016, PhRvL, 116, 241103
 Berger E., 2014, ARA&A, 52, 43
 Bromberg O., Nakar E., Piran T., Sari R., 2011, ApJ, 740, 100
 Cavallo G., Rees M. J., 1978, MNRAS, 183, 359
 Chhotray A., Lazzati D., 2017, arXiv, arXiv:1705.03469
 De Colle F., Lu W., Kumar P., Ramirez-Ruiz E., Smoot G., 2017, arXiv, arXiv:1701.05198
 Eichler D., Livio M., Piran T., Schramm D. N., 1989, Natur, 340, 126
 Faber J. A., Rasio F. A., 2002, PhRvD, 65, 084042
 Faber J. A., Baumgarte T. W., Shapiro S. L., Taniguchi K., 2006, ApJ, 641, L93
 Fong W., Berger E., 2013, ApJ, 776, 18
 Fong W., Berger E., Margutti R., Zauderer B. A., 2015, ApJ, 815, 102
 Ghirlanda G., et al., 2015, A&A, 578, A71
 Ghirlanda G., et al., 2016, arXiv, arXiv:1607.07875
 Giacomazzo B., Perna R., Rezzolla L., Troja E., Lazzati D., 2013, ApJ, 762, L18
 Goodman J., 1986, ApJ, 308, L47
 Gottlieb O., Nakar E., Piran T., 2017, arXiv, arXiv:1705.10797
 Granot J., Panaitescu A., Kumar P., Woosley S. E., 2002, ApJ, 570, L61
 Greiner J., Hartmann D. H., Voges W., Boller T., Schwarz R., Zharikov S. V., 2000, A&A, 353, 998
 Guidorzi C., et al., 2009, A&A, 499, 439
 Kasen D., Fernández R., Metzger B. D., 2015, MNRAS, 450, 1777
 Kisaka S., Ioka K., Takami H., 2015, ApJ, 802, 119
 Kisaka S., Ioka K., Nakamura T., 2015, ApJ, 809, L8
 Kiuchi K., Kyutoku K., Sekiguchi Y., Shibata M., Wada T., 2014, PhRvD, 90, 041502
 Kiuchi K., Sekiguchi Y., Kyutoku K., Shibata M., Taniguchi K., Wada T., 2015, PhRvD, 92, 064034
 Lazzati D., Begelman M. C., 2005, ApJ, 629, 903
 Lazzati D., Morsony B. J., Begelman M. C., 2010, ApJ, 717, 239
 Lazzati D., Morsony B. J., Blackwell C. H., Begelman M. C., 2012, ApJ, 750, 68
 Lazzati D., 2016, arXiv, arXiv:1605.03617
 Li L.-X., Paczyński B., 1998, ApJ, 507, L59
 Li X., Hu Y.-M., Fan Y.-Z., Wei D.-M., 2016, ApJ, 827, 75
 Matzner C. D., 2003, MNRAS, 345, 575
 Mészáros P., Rees M. J., 2000, ApJ, 530, 292
 Metzger B. D., et al., 2010, MNRAS, 406, 2650
 Metzger B. D., Berger E., 2012, ApJ, 746, 48
 Metzger B. D., Bauswein A., Goriely S., Kasen D., 2015, MNRAS, 446, 1115
 Morsony B. J., Lazzati D., Begelman M. C., 2007, ApJ, 665, 569
 Morsony B. J., Workman J. C., Ryan D. M., 2016, ApJ, 825, L24
 Nakar E., Piran T., Granot J., 2002, ApJ, 579, 699
 Nakar E., 2007, PhR, 442, 166
 Nakar E., Piran T., 2017, ApJ, 834, 28
 Narayan R., Kumar P., 2009, MNRAS, 394, L117
 Phinney E. S., 1991, ApJ, 380, L17
 Radice D., Galeazzi F., Lippuner J., Roberts L. F., Ott C. D., Rezzolla L., 2016, MNRAS, 460, 3255
 Ramirez-Ruiz E., Celotti A., Rees M. J., 2002, MNRAS, 337, 1349
 Rau A., Greiner J., 2005, NCimC, 28, 327
 Rau A., Greiner J., Schwarz R., 2006, A&A, 449, 79
 Rhoads J. E., 1999, ApJ, 525, 737
 Rossi E. M., Lazzati D., Salmonson J. D., Ghisellini G., 2004, MNRAS, 354, 86
 Rossi E. M., Perna R., Daigne F., 2008, MNRAS, 390, 675
 Ruiz M., Lang R. N., Paschalidis V., Shapiro S. L., 2016, ApJ, 824, L6
 Rykoff E. S., et al., 2005, ApJ, 631, 1032
 Salafia O. S., Ghisellini G., Pescalli A., Ghirlanda G., Nappo F., 2015, MNRAS, 450, 3549
 Salafia O. S., Ghisellini G., Pescalli A., Ghirlanda G., Nappo F., 2016, MNRAS, 461, 3607
 Sekiguchi Y., Kiuchi K., Kyutoku K., Shibata M., 2011, PhRvL, 107, 051102
 Shibata M., Uryū K., 2002, PThPh, 107, 265
 Shibata M., Taniguchi K., 2006, PhRvD, 73, 064027
 van Eerten H., Zhang W., MacFadyen A., 2010, ApJ, 722, 235
 Yamazaki R., Ioka K., Nakamura T., 2002, ApJ, 571, L31
 Yamazaki R., Ioka K., Nakamura T., 2003, ApJ, 591, 283
 Yamazaki R., Yonetoku D., Nakamura T., 2003, ApJ, 594, L79
 Zhang B., Yan H., 2011, ApJ, 726, 90